PCCP

Accepted Manuscript

ROYAL SOCIETY OF CHEMISTRY

www.rsc.org/pccp

ARTICLE TYPE www. rsc.org/xxxxxx | XXXXXXXX

Curie-type paramagnetic NMR relaxation in the aqueous solution of Ni(II)

Jiří Mareš,[a] Matti Hanni,[a,b] Perttu Lantto,[a] Juhani Lounila,[a] and Juha Vaara[a]

Received Xth XXXXXXXXXX 20XX, Accepted Xth XXXXXXXXX 20XX
First published on the web Xth XXXXXXXXXX 200X
DOI: 10.1039/b000000x ***Received Xth XXXXXXXXXX 20XX, Accepted Xth XXXXXXXXX 20XX***

First published on the web Xth XXXXXXXXXX 200X
DOI: 10.1039/b000000x

$Ni^{2+}(aq)$ has been used for many decades as a model system for paramagnetic nuclear magnetic resonance (pNMR) relaxation studies. More recently, its magnetic properties and also nuclear magnetic relaxation rates have been studied computationally. We have calculated electron paramagnetic resonance and NMR parameters using quantum-mechanical (QM) computation of molecular dynamics snapshots, obtained using a polarizable empirical force field. Statistical averages of hyperfine coupling, g- and zero-field splitting tensors, as well as the pNMR shielding terms, are compared to the available experimental and computational data. In accordance with our previous work, the isotropic hyperfine coupling as well as nuclear shielding values agree well with experimental measurements for the ^{17}O nuclei of water molecules in the first solvation shell of the nickel ion, whereas larger deviations are found for ^{1}H centers. We report, for the first time, the Curie-type contribution to the pNMR relaxation rate using QM calculations together with Redfield relaxation theory. The Curie relaxation mechanism is analogous to chemical shift anisotropy relaxation, well-known in diamagnetic NMR. Due to the predominance of other types of paramagnetic relaxation mechanisms for this system, the Curie term is only possible to extract computationally. The Curie mechanism alone would result in around 16 and 20 s^{-1} of relaxation rate (R_1 and R_2 respectively) for the ^{1}H nuclei of water molecules bonded to the Ni^{2+} center, in a magnetic field of 11.7 T. The corresponding ^{17}O relaxation rates are around 33 and 38 s^{-1}. We also report the Curie contribution to the relaxation rate for molecules beyond the first solvation shell in a 1 M solution of Ni^{2+} in water.

1 Introduction

The NMR relaxation process involves phenomena belonging to a number of different physical disciplines. A purely computational approach to NMR relaxation has to span accurate modeling of molecular structures, dynamics as well as electronic-structure calculation of molecular property parameters involved in the Hamiltonian of relevance for the studied relaxation mechanism. To that one has to add an appropriate treatment of the nuclear spin system.[1] The calculation of relaxation rates due to fluctuation of a first-order molecular property, such as the electric-field gradient in quadrupolar relaxation, has reached a mature level with good agreement with the experimental results in various chemical environments and phases of materials.[2] In contrast, only recently a close agreement between first-principles computational and experimental results was obtained in a case where second-order property — chemical shift anisotropy (CSA) — provides the dominant relaxation mechanism.[3] This was the case in a study pursued on a diamagnetic monoatomic xenon gas, where a fluctuating CSA is produced predominantly by atomic collisions. In the case of paramagnetic substances, the dominant NMR relaxation mechanisms are connected with the strong magnetic moment of the unpaired electron(s) and its coupling to the adjacent nuclear magnetic moments. In some cases, the strength of the interaction and the relation of the relevant correlation and relaxation times do not allow to use a perturbation theory-based relaxation treatment.[4–13] For appropriate theoretical analysis of the experimental data in such cases, the well-known Swedish slow-motion theory was developed[8] in parallel with the Florence theory (see, *e.g.*, Ref.[14]). The work of Odelius, Ribbing and Kowalewski[15] pioneered by pursuing a fully computational approach to electron spin relaxation, combining molecular dynamics (MD) simulation and quantum mechanical (QM) calculation of the EPR Hamiltonian parameters from the MD snaphots, together with a spin dynamic simulations. The obtained electronic relaxation rate was then used to estimate ^{1}H relaxation rates.

[a] *NMR Research Group, Department of Physics, University of Oulu, P.O. Box 3000, FIN-90014, Oulu, Finland. Fax: +358-(0)8-553 1287; E-mail: jiri.mares@oulu.fi, juha.vaara@iki.fi*
[b] *Department of Radiology, University of Oulu, P.O. Box 5000, FIN-90014, Oulu, Finland*

The paramagnetic relaxation enhancement is in general caused by the fluctuating interaction of electronic and nuclear magnetic moments. The expression for this interaction Hamiltonian is

$$H = \mathbf{S} \cdot \mathbf{A} \cdot \mathbf{I}, \quad (1)$$

where **S** and **I** are the electron and nuclear spin vectors and **A** is the hyperfine coupling tensor. Via H the nuclear spin experiences a time-dependent interaction, which can somewhat arbitrarily be divided to, on the one hand, the fast fluctuations of **S** between its quantum-mechanical states and, on the other hand, the slow, molecular dynamics-induced fluctuations of the so-called Curie spin S_C, which results from the average over the electronic fluctuations. In particular, component of the Curie spin along the external magnetic field is[16]

$$\langle S_z \rangle = \frac{B_0}{3kT} g_e \mu_B S(S+1). \quad (2)$$

The paramagnetic nuclear shielding terms $\boldsymbol{\sigma}$ in the NMR spin Hamiltonian arise from the hyperfine interaction of the nuclei with the average Curie spin.[17] In a similar vein, fluctuation of the nuclear shielding due to molecular motions causes, in turn, nuclear spin relaxation analogous to the CSA relaxation of the diamagnetic systems.

In this work we concentrate on the Curie relaxation caused by this average spin.[18,19] In modern theory the average spin is considered via a second rank dyadic,[20] in the necessary generalisation of the doublet-like (effective spin quantum number $S = \frac{1}{2}$) treatment[21,22] for $S \geq 1$ systems such as the prototypic Ni^{2+} ($S = 1$). To calculate the relaxation time associated with the Curie mechanism, it is natural to employ the novel theory for pNMR shielding and also make use of the analogy with the diamagnetic CSA relaxation. We employ the perturbation Redfield theory[4,5] for this purpose. The Curie-type relaxation mechanism is typically found important for big molecules with large effective spin, at high magnetic fields.[18] Its importance is also recognised for lanthanide ions.[16] In this work we choose the $Ni^{2+}(aq)$ system to computationally investigate the modeling methodology necessary in the context of Curie-type relaxation. This simple system of prototypic nature already features a rich phenomenology.

2 Methods

2.1 Molecular dynamics simulation

One Ni^{2+} ion and 464 water molecules were simulated in a periodic cubic box with 24.044 Å side-length [average dimension from the equilibrated constant pressure and temperature (NPT) simulation] using the AMOEBA polarizable forcefield in the Tinker MD package.[23] After equilibration at 300 K and 1 atm, the production dynamics continued in the constant volume and energy (NVE) ensemble resulting in a total of 0.95 ns of trajectory during which the running average temperature drifted by less than 0.5 K.[24]

2.2 Snapshot extraction

For the snapshot calculations, roughly spherical water clusters centered around the Ni^{2+} ion were extracted from the simulation box. Whereas for the zero-field splitting (ZFS) and g-tensor calculations only the first solvation shell consisting of six water molecules was included, the hyperfine coupling (HFC) tensors were calculated for larger clusters consisting of the first and second solvation shells, and the third shell was included as an explicit solvation layer. The set of snapshot clusters was extracted from the first 0.75 ns section of the 0.95 ns of the equilibrated trajectory, sampled every 240 fs resulting in 3125 snapshots.

2.3 Quantum mechanical calculations

The HFC, g, and ZFS-tensor calculations from the snapshots of the MD trajectory were carried out in the ORCA program.[25–28] The g-tensor calculations were carried out on the unrestricted Kohn-Sham density-functional theory (DFT) level using the PBE functional[29] together with the resolution-of-identity approximation[30] and def2-TZVP basis set.[31]

The ZFS tensors were calculated at the N-electron valence state perturbation theory (NEVPT2) level[32–34] as implemented in the ORCA programme, using the def2-TZVP basis set. The active space of the underlying state-averaged complete active space self-consistent field (CASSCF) calculation consisted of eight electrons in five orbitals as appropriate for ligand field theory for a d^8 metal in an (on average) octahedral coordination. All 10 triplets and 15 singlet states allowed by the CASSCF(8,5) calculation were included. The same method for the same system was employed by Kubica *et al.*[35]

For calculation of the HFC tensors, the (15s 11p 6d)/[9s 7p 4d] basis by Munzarová and Kaupp[36] was used for the nickel ion, whereas the aug-pcJ-1 basis[37] was used for the light atoms belonging to the first and second solvation shells. The HFCs were evaluated with an explicit solvation shell consisting of water molecules of the third solvation shell employing the SVP basis.[38] The pNMR shielding term analysis was obtained according to the theory of Pennanen and Vaara.[20]

We showed previously[39] that the described level of theory is required for the HFC tensor calculations and that both the first and the second solvation shells should be calculated by QM methods. Only at larger distances the point-dipole approximation is safely valid for this system. The level of calculation of ZFS was chosen according to the recent investigation of Kubica *et al.*[35] Further details follow in the Results and Discus-

sion section. The g-tensor calculation showed little influence of the solvating molecules beyond the first shell. The chosen method was economical for obtaining a large number of MD snapshots.

2.4 pNMR shielding

For the theory of pNMR shielding, see Ref.[20]. For the sake of completeness, we briefly review the shielding expression

$$\boldsymbol{\sigma} = \boldsymbol{\sigma}_{\mathrm{orb}} - \frac{\mu_{\mathrm{B}}}{\gamma kT}\, \boldsymbol{g} \cdot \langle \boldsymbol{SS} \rangle_0 \cdot \boldsymbol{A} \tag{3}$$

$$\langle \boldsymbol{SS} \rangle_0 = \frac{\sum_n \langle n|\boldsymbol{SS}|n\rangle \exp[-E_n(0)/kT]}{\sum_n \exp[-E_n(0)/kT]}, \tag{4}$$

in which $\boldsymbol{\sigma}_{\mathrm{orb}}$ is the (approximately) temperature-independent orbital shielding.[17,40] The second term contains the product of the g-tensor, the dyadic $\langle \boldsymbol{SS} \rangle_0$ of the effective spin operator $\boldsymbol{S}$ thermally averaged in the ZFS-split groundstate manifold of the magnetic sublevels $|n\rangle$, and the HFC tensor $\boldsymbol{A}$. The factors k and T stand for the Boltzmann constant and the absolute temperature, respectively. An assumption underlying the Boltzmann averages[21] is that the electron spin relaxation is much faster than nuclear spin relaxation, rendering the electronic transitions instrumental in determining the equilibrium population of the states $|n\rangle$. Hence, the nuclear spin interacts with the average Curie spin.

We analyze the hyperfine part of the shielding expression by performing a break-down of $\boldsymbol{g}$ and $\boldsymbol{A}$ to the leading-order terms involving also the leading-order corrections arising from the spin-orbit (SO) interactions.[20–22,41] The HFC tensor can be decomposed as

$$\boldsymbol{A} = A_{\mathrm{con}}\mathbf{1} + \boldsymbol{A}_{\mathrm{dip}} + A_{\mathrm{PC}}\mathbf{1} + \boldsymbol{A}_{\mathrm{dip,2}} + \boldsymbol{A}_{\mathrm{as}} \tag{5}$$

where the first two terms on the right-hand side are the nonrelativistic, isotropic contact and anisotropic dipolar couplings, respectively. $A_{\mathrm{PC}}\mathbf{1}$ is the isotropic pseudocontact term that, along with the anisotropic symmetric (dip,2) and antisymmetric (as) contributions, arise due to the relativistic SO correction to HFC.[42] The g-tensor can be decomposed as

$$\boldsymbol{g} = (g_e + \Delta g_{\mathrm{iso}})\mathbf{1} + \Delta\tilde{\boldsymbol{g}} \tag{6}$$

where g_e is the free electron factor, Δg is the isotropic and $\Delta\tilde{\boldsymbol{g}}$ the anisotropic part of the g shift tensor. The contributions to the total shielding resulting from the combinations of $\boldsymbol{g}$ and $\boldsymbol{A}$ broken down into the various contributions, are listed in Table 1.

2.5 Curie relaxation within the Redfield relaxation theory

Since Curie relaxation is caused by the interaction of nuclear spin with the fluctuating Curie spin of the molecule, the relevant Hamiltonian of the interaction is the term involving the nuclear shielding from the NMR spin Hamiltonian. This leads to a formulation of the Curie relaxation fully analogous to the CSA relaxation of diamagnetic systems. Consequently, from the Redfield relaxation theory, the "spin-lattice" and "spin-spin" relaxation rates are obtained as

$$R_1 = \frac{1}{2}\omega_0^2 J(\omega_0) \tag{7}$$

$$R_2 = \frac{1}{12}\omega_0^2 [4J(0) + 3J(\omega_0)], \tag{8}$$

where $J(\omega)$ is the spectral density function and ω_0 is the Larmor frequency of the corresponding nucleus obtained as $\omega_0 = \gamma B_0$. It is worth noting that the relaxation rate increases quadratically with the magnetic field in the regime where $J(\omega_0) \simeq J(0)$.[1] The expression for the spectral density function reads

$$J(\omega) = 2Re\left\{ \int_0^\infty \langle \sigma_{2,0}(t)\sigma_{2,0}(t+\tau)\rangle e^{-i\omega\tau} d\tau \right\}, \tag{9}$$

with $\sigma_{2,0} = (2\sigma_{zz} - \sigma_{xx} - \sigma_{yy})/\sqrt{6}$ the irreducible $l = 2, q = 0$ spherical component of the shielding tensor, where the z axis is along the external magnetic field B_0. $\langle \sigma_{2,0}(t)\sigma_{2,0}(t+\tau)\rangle$ is approximated in the present work by the combination of MD simulations and quantum-mechanical snaphot calculations, leading to a series of instantaneous $\boldsymbol{\sigma}$ values for ^{1}H and ^{17}O nuclei.

3 Results and discussion

3.1 Static EPR/NMR properties

The calculations largely follow our previous work,[39] where we extensively tested the available methods for the EPR parameters and NMR shielding against the experimental data. Where the experimental reference point is not available, the range of results obtained by the different methods can serve as an error estimate. The difference between the approach of Ref.[39] and the current paper is, on the one hand, in the MD method that was used to obtain the trajectory sampled in the QM snapshot calculations. On the other hand, a more accurate method was used presently for the ZFS calculations. Briefly, in the previous work (Ref.[39]), the MD trajectory was obtained by a first-principles MD method using mixed Gaussian orbital/plane wave basis set and the PBE exchange-correlation functional of DFT, which provided sufficiently accurate structures of the molecular complex. However, the dynamical properties, *e.g.*, the rotational correlation times or the translational diffusion coefficient were found to be unacceptable at that level. In this work, we use the AMOEBA forcefield, with an accurately parameterised Ni-H_2O potential, with the result

Table 1 Contributions to the irreducible $l = 2$, $q = 0$ spherical component of the shielding tensor [a] of ^{1}H and ^{17}O from different physical mechanisms, simulated for atoms in the first and second solvation shell of the aqueous solution of the Ni^{2+} ion.

				Contributions to $S = 1$ [b]			Numerical results (ppm) for solution of Ni^{2+} [c]			
Term name	Term in $\sigma_{\varepsilon\tau}$	Number	Order	rank-0	rank-1	rank-2	FSS/^{1}H	SSS/^{1}H	FSS/^{17}O	SSS/^{17}O
σ_{orb} [d]	σ_{orb}	0	$\mathcal{O}(\alpha^2)$	x	x	x	-	-	-	-
σ_{con} [e]	$g_e A_{con}\langle S_\varepsilon S_\tau\rangle_0$	1	$\mathcal{O}(\alpha^2)$	x	-	x	1.50	0.0364	131	1.78
σ_{dip}	$g_e \sum_b A^{dip}_{b\tau}\langle S_\varepsilon S_b\rangle_0$	2	$\mathcal{O}(\alpha^2)$	x	x	x	304	63.3	2673	93.2
$\sigma_{con,2}$	$g_e A_{PC}\langle S_\varepsilon S_\tau\rangle_0$	3	$\mathcal{O}(\alpha^4)$	x	-	x	0.0182	0.000959	1.08	0.00694
$\sigma_{dip,2}$	$g_e \sum_b A^{dip,2}_{b\tau}\langle S_\varepsilon S_b\rangle_0$	4	$\mathcal{O}(\alpha^4)$	x	x	x	14.1	3.00	109	3.14
σ_{ac}	$g_e \sum_b A^{as}_{b\tau}\langle S_\varepsilon S_b\rangle_0$	5	$\mathcal{O}(\alpha^4)$	-	x	x	0.0153	0.00176	0.139	0.00628
$\sigma_{con,3}$	$\Delta g_{iso} A_{con}\langle S_\varepsilon S_\tau\rangle_0$	6	$\mathcal{O}(\alpha^4)$	x	-	x	0.0765	0.001835	6.68	0.0904
$\sigma_{dip,3}$	$\Delta g_{iso} \sum_b A^{dip}_{b\tau}\langle S_\varepsilon S_b\rangle_0$	7	$\mathcal{O}(\alpha^4)$	x	x	x	15.1	3.15	133	4.65
$\sigma_{c,aniso}$	$A_{con} \sum_a \Delta\tilde{g}_{\varepsilon a}\langle S_a S_\tau\rangle_0$	8	$\mathcal{O}(\alpha^4)$	x	x	x	0.369	0.00908	33.2	0.441
σ_{pc}	$\sum_{ab} \Delta\tilde{g}_{\varepsilon a} A^{dip}_{b\tau}\langle S_a S_b\rangle_0$	9	$\mathcal{O}(\alpha^4)$	x	x	x	0.518	0.100	4.89	0.146

[a] The component is defined the same way as in eq. (9), the presented values are root-mean squares of the 3125 snapshots sampled every 240 fs from the MD trajectory. [b] Rank-0, 2, and 1 contributions correspond to the isotropic shielding constant and anisotropic symmetric, as well as antisymmetric terms, respectively. [c] Only contribution to first solvation shell (FSS) and second solvation shell (SSS) are presented. FSS is formed by six water molecules bonded to Ni^{2+}, whereas SSS is formed by water molecules that have at least one atom within 5 Å from the Ni^{2+} ion. [d] Orbital shielding is not relevant for this work and therefore not calculated. [e] $g_e \doteq 2.002319$ is the free-electron g-value.

that both structural and dynamical properties of $Ni^{2+}(aq)$ are accurately modeled.

Concerning the choice of method for the calculation of the ZFS tensors, we chose here the *ab initio* NEVPT2 method probed for this system also in Ref.[35], which also showed the drawbacks of the previously employed, DFT-based calculation of ZFS.

The results of the QM calculations of the static EPR/NMR parameters are gathered in Table 2. We compare results obtained in this work with our previous paper and estimate at the same time the implied inaccuracy for the subsequent Curie-type relaxation calculations.

3.1.1 *g*-tensor

The present results for the g-tensor are very similar to results in our previous work (Ref.[39]). Also differences among results for this parameter obtained by different DFT functionals are generally small. From four of the nuclear shielding terms (Table 1), in which the deviation of the g-tensor from the free electron values appears,[20] only one ($\sigma_{dip,3}$) gives a non-negligible contribution to the relaxation rate. The inaccuracy of the calculations of the g-tensor introduces an error of the relaxation rate of at most a few percent.

3.1.2 Zero-field splitting tensor

The results for the ZFS-tensors changed very significantly as compared to the earlier paper. In the previous DFT calculations, the values suffered from the dependence on the system size, as explained in Ref.[43]. Regardless of this specific problem, it was shown by Kubica *et al.*[35] that DFT-based calculation of the ZFS tensor is highly unreliable for nickel complexes. Therefore, in the current work we used an *ab initio* method which was demonstrated to be superior in the cited work. The comparison of the calculated root-mean square scalar quantity that can be calculated from the components of the traceless ZFS tensor, $\Delta_5 = \sqrt{\langle \boldsymbol{D} : \boldsymbol{D}\rangle/5} = 3.5$ cm^{-1} with the experimental values ($\Delta_5 = 2.6$ and 3.0 cm^{-1} in Refs.[44] and[9], respectively) now shows a reasonable agreement (see also Table 2). Although the D and E values of the ZFS tensor can be calculated for individual snaphots, in the — on average — hexagonally symmetric complex, they average to zero, and can not be experimentally observed. Figure 1 shows the time autocorrelation function $\langle \boldsymbol{D}(0) : \boldsymbol{D}(\tau)\rangle$ featuring a fast and a much slower component of decay. Since the ZFS-tensor enters the calculation of the nuclear shielding tensor only indirectly, the resulting shielding values in this work and the previous paper[39] are rather similar, despite large changes in the ZFS itself. In particular, the isotropic shielding constant remains practically unaffected. On the other hand, with the two to three orders of magnitude higher values of the Δ_5 (as presented in Ref.[39]), the resulting shielding anisotropy results would be 4% and 1% higher for ^{1}H and ^{17}O, respectively, than what is obtained presently. On account of its quadratic dependence on the anisotropy of the paramagnetic shielding tensor, the corresponding Curie-type relaxation would be 8% and 2% faster for such overestimated ZFS.

3.1.3 Hyperfine coupling tensor

Since the rank-0 part of the HFC-tensor - the hyperfine coupling constant - is strongly dependent on the geometry of the paramagnetic complex, the results based on the differently obtained MD trajectories in this work and in Ref.[39] differ significantly. This probably reflects more the uncertainties of DFT calculations of HFC than represents a sign of inaccuracy of the MD trajectory. Specifically, DFT-based HFC constant (Ref.[39]) as well as the diamagnetic shielding and indirect spin-spin coupling constants (Ref.[45]) appear to be more reliable when calculated from structures obtained by the same DFT functional as used for calculating the hyperfine property. This is not the case in the present empirical MD/QM procedure, however. Consequently, the magnitude of the average

hyperfine coupling constant is around three times larger for ^{1}H and 30% larger for ^{17}O in the current work as compared to results calculated by the corresponding method in our previous work. For the ^{1}H centers, both the present results and those of Ref.[39] are far from the available experimental data, whereas for ^{17}O, the agreement with the experimental results is rather good, considering the differences between the experimental conditions and our simulations (see also the footnotes of Table 2). The HFC constant will influence the rank-2 parts of the shielding tensors only negligibly via terms 1, 6 and 8 in the shielding expression (Table 1), therefore this inaccuracy (especially for the ^{1}H nuclei) is irrelevant for the nuclear relaxation rates.

The second-rank part of the HFC tensor $\boldsymbol{A}^{\mathrm{dip}}$ has by far the largest and most direct impact on Curie-type relaxation. The span of the largest eigenvalue of the dipolar HFC, A_{33}^{dip}, obtained in Ref.[39] (values in the 7.5–8.75 MHz range obtained with the different DFT functionals) provides the most conservative error estimate of $\sim$15% for this parameter in the case of ^{1}H. The components of the HFC tensor appear linearly in the equation (3) for nuclear shielding, but are squared in the calculation of the time correlation functions and the spectral density function [eq. (9)]. The maximum error in the Curie relaxation rate due to the variation of the second rank-part of HFC is thus $\sim$30% in the case of ^{1}H. Furthermore, for ^{1}H, the point-dipole approximation was shown to be valid for atoms beyond the second solvation shell (Ref.[39]). The calculation of this contribution for nuclei that are distant from the paramagnetic center is, therefore, also reliable.

The situation for the ^{17}O nuclei is less favourable, as the differences between the results obtained by the different computational methods are rather large, which can in the most conservative estimate result in an error of the Curie relaxation rate of the order of tens of percent.

3.2 Curie relaxation

Within the Redfield theory,[4,5] only the second-rank spherical components of the shielding tensor are considered. In principle all the nine different terms of the hyperfine part of the pNMR shielding expression (including the contact shielding) contain second-rank contributions for systems of higher spin than $\frac{1}{2}$.[20] All of them can, therefore, contribute to the relaxation rate. In practice, however, only the three terms that contain the dipolar part of the hyperfine coupling tensor, contribute by a numerically significant amount in the present example system, the aqueous solution of Ni^{2+}. The resulting Curie relaxation rates are listed in Table 3 for the field strength of 11.7 T. The required time correlation functions of the zeroth component of the second-rank spherical tensor of the total hyperfine shielding are plotted in Figures 2 and 3 for the first solvation shell of Ni^{2+} and bulk water, respectively. Based on test calculations with reduced lengths of the MD trajectory (as compared to the full trajectory), the oscillations in the time correlation functions that start after $\tau \simeq 50$ ps can be considered as noise due to insufficient statistics, which is more severe for the atoms of the first solvation shell (six molecules) than for the atoms of the other molecules (458 molecules). Therefore, our results for the relaxation rates are obtained by replacing the original simulated data points beyond ca. 50 ps by a fitted bi-/tri-exponential curve, as shown in Figures 2 and 3. The resulting data was Fourier-transformed [eq. (9)] before using in the calculation of the relaxation rates.

The resulting spectral density functions (Figures 4 and 5) show the interaction strength that is available for a given frequency. The relevant frequencies in the Redfield theory expression are either the Larmor frequency or zero (eqs. 7, 8). We can see that, for our system, the spectral density at the Larmor frequency of ^{1}H differs from spectral density at zero frequency. A similar value would have indicated residing within the regime of the so-called extreme narrowing limit.[46] In contrast, this regime is still well valid for the ^{17}O nuclei. The extreme narrowing limit extends over a much wider range of Larmor frequencies for gaseous samples, such as Xe gas.[3] Within this regime, the CSA and Curie relaxation rates have within the Redfield theory a quadratic dependence on the magnetic field as the spectral density function remains constant. On the other hand, in the example high-field calculation in section 3.2.2 below, the spectral density $J(\omega_0)$ is far from $J(0)$. In that case the R_2 relaxation rate still preserves a component of quadratic dependence on the magnetic field due to $J(0)$, whereas the R_1 relaxation rate grows slower.

Along with the spectral density functions, Figures 4 and 5 show also their Lorentzian fits. These would correspond to a single-exponential decay of the correlation function, and are shown only for comparison.

3.2.1 First-shell and bulk relaxation rates

Table 3 lists the average Curie relaxation rates for the ^{1}H and ^{17}O atoms in the first solvation shell of Ni^{2+} and in bulk water. The first shell is a stable entity in the timescale of the present simulation, whereas the "bulk" includes all molecules within the second shell and further from the central ion. To reduce the dependence of the results on the size of the simulation box, which determines the concentration of the Ni^{2+} ions, the bulk relaxation rates were recalculated for a 1 M Ni^{2+} solution. On the other hand, the term relaxivity is commonly defined as an increase of the relaxation rate due to 1 mM concentration of the relaxation substance, hence our scale is 1000$\times$ larger.

For simplicity we assume that there is a fast exchange from and to the first solvation shell in the timescale of NMR relaxation. Consequently, in the aqueous solution of Ni^{2+}, the average calculated R_1 relaxation rate due to Curie relaxation can be calculated by noting that 1 litre of 1 M Ni^{2+} solution contains

6 mol of the first-shell water molecules and roughly 55 mol of water molecules altogether. Taking the simulated value of 16 s^{-1} for ^{1}H R_1 in the first solvation shell from Table 3, the corresponding contributions to the average relaxation rate in 1 M solution is $16 \times \frac{6}{55} \doteq 1.7\ s^{-1}$. The average contribution of the second shell and more distant atoms is directly presented in Table 3. Assuming a simple additivity, in 1 M solution the ^{1}H R_1 relaxation rate would be $(1.7 + 0.45)\ s^{-1} \doteq 2.2\ s^{-1}$. Relaxation rates obtained in this way are listed in Table 3.

The molecules in the first solvation shell contribute generally more to the relaxation rate of the whole solution than the molecules outside the first solvation shell. In the 1 M solution the contribution of the first solvation shell is roughly four times that of the bulk molecules for ^{1}H nuclei, whereas for the ^{17}O nuclei, the corresponding ratio is more than 250.

3.2.2 Significance of Curie-type relaxation

There are obvious reasons why the Curie relaxation accounts only for a small part of the total relaxation rate. Investigation of the magnitude of the pNMR Hamiltonian terms acting on the nuclear spin, the hyperfine coupling of the fluctuating electron spin with the nuclear spin is much larger than the interaction with the average Curie spin, represented by the shielding Hamiltonian. Therefore, the former interaction accounts for the major contribution to the NMR relaxation rate. However, similarly to diamagnetic CSA relaxation,[47] experimentally the presence of Curie relaxation can be readily identified due to its strong (quadratic in the fast-motion regime) dependence on the magnetic field, as seen from the nuclear magnetic relaxation dispersion (NMRD) profiles. In this way, the Curie relaxation has been seen for several lanthanide ions,[48] whereas the NMRD curves of Ni^{2+} solution do not show the characteristic magnetic field dependence.[9] Computations are therefore essential in providing an estimate of the magnitude of this contribution.

The Curie relaxation rate of 2.2 s^{-1} for ^{1}H in $Ni^{2+}(aq)$ as above, can be compared with the experimental total relaxation rate of 7100 s^{-1} (324 K, 1 M).[9] Neglecting the difference in temperature, the Curie relaxation contributes by as little as 0.031% to the total ^{1}H relaxation rate at the magnetic field of 11.7 T. For comparison, in the entirely hypothetical magnetic field of 1000 T, the Curie contribution to the ^{1}H R_1 relaxation rate would reach ca. 140 s^{-1} and 1×10^4 s^{-1} for R_2 (1 M solution).

We note that the R_1 and R_2 relaxation rates of ^{17}O due to quadrupolar interaction are both as fast as 150 s^{-1} at room temperature and at the magnetic field of 1.4 T.[49]

3.2.3 Validity of the Redfield theory

Paramagnetic Ni^{2+} causes a hyperfine contribution to the nuclear shielding, responsible for Curie relaxation. This contribution is in the first solvation shell around two orders of magnitude larger than the orbital shielding in diamagnetic molecules. Despite this fact the requirements for the perturbational Redfield relaxation theory remain very well fulfilled for the Curie mechanism. In particular, the correlation time of the pNMR shielding Hamiltonian, ca. 17 ps for the first-shell ^{1}H nuclei (Figure 2), is much shorter than the Curie relaxation time (tens of milliseconds or longer, Table 3). The same comparison for ^{17}O (correlation time of ca. 20 ps) gives a similar order of magnitude for the separation between the relevant correlation and relaxation times. The other, related, requirement is that in the interaction picture, the time-dependent perturbation Hamiltonian is sufficiently small. The combined condition is often written as

$$\omega_H \tau_c \ll 1 \tag{10}$$

where ω_H denotes the root-mean square interacting Hamiltonian in frequency units and τ_c the correlation time of the pNMR shielding Hamiltonian, as discussed above. For ^{1}H in the magnetic field of 11.7 T the condition evaluates as $\omega_H \tau_c \simeq 17 \times 10^{-6} \ll 1$. *

4 Conclusions

We have investigated the contributions to the paramagnetic nuclear spin relaxation enhancement in the prototypic system of $Ni^{2+}(aq)$ due to the Curie-type relaxation mechanism, using computational methods.

The necessary steps involved were (1) molecular dynamics simulation, (2) snapshot extraction and quantum-mechanical calculation of the EPR parameters, (3) calculation of the instantaneous pNMR shielding tensors using modern non-doublet theory, (4) calculation of the time-correlation functions of irreducible spherical components of the shielding tensors, (5) calculation of the spectral density functions, and finally (6) applying the equations of the Redfield relaxation theory identical to those of the CSA relaxation in diamagnetic systems, to obtain the Curie contribution to the relaxation rates.

The spherical $\sigma_{2,0}$ component of the dipolar pNMR shielding tensor makes the by far dominant contribution to the Curie-type relaxation in the studied system. $\sigma_{2,0}$ can be calculated with sufficient accuracy and efficiency using DFT methods, apart from the demanding ZFS tensor. For ZFS, we chose to use a state-of-the-art *ab initio* method. The Curie relaxation is estimated to contribute by 16 s^{-1} for R_1 and 20 s^{-1} for R_2 to ^{1}H relaxation rates of water molecules in the first solvation shell of the Ni^{2+} ion at 11.7 T magnetic field. For ^{17}O,

* Inserting a value of $\sqrt{(110000 ppm^2)} \simeq 330$ ppm for $\langle \sigma_{2,0} \rangle$ (Fig. 2) into $\omega_H = \langle \sigma_{2,0} \rangle \gamma_{^1H} B_0$ yields $\omega_H \simeq 1 \times 10^6$ rad/s. Then $\omega_H \tau_c \simeq 1 \times 10^6 \cdot 17 \times 10^{-12} = 17 \times 10^{-6} \ll 1$.

Table 3 Simulated Curie-type nuclear spin relaxation contributions (in s^{-1}) for ^{1}H and ^{17}O nuclei of water molecules in the first solvation shell (FSS) of the aqueous solution of Ni^{2+} as well as the bulk solution. The notation is R_1; R_2. The numbers are calculated from 3125 snapshots sampled over 0.75 ns of molecular dynamics trajectory. Paramagnetic shielding was obtained using the formal temperature of 300 K and the magnetic field was set to 11.7 T. All values for the bulk molecules are recalculated to the concentration of the Ni^{2+} ion of 1 M.[a]

Shielding term [b]	R_1; R_2 for nucleus (shell)					
	^{1}H (FSS)	^{1}H (bulk)	^{1}H (1 M total) [c]	^{17}O (FSS)	^{17}O (bulk)	^{17}O (1 M total)[c]
σ_{dip}	13; 17	0.30; 0.41	1.7; 2.3	26; 30	0.012; 0.014	2.8; 3.3
$\sigma_{dip,2}$	0.032; 0.042	3.2×10^{-4}; 3.9×10^{-4}	3.8×10^{-3}; 5.0×10^{-3}	0.037; 0.043	7.4×10^{-6}; 8.7×10^{-6}	4.0×10^{-3}; 4.7×10^{-3}
$\sigma_{dip,3}$	0.032; 0.041	7.6×10^{-4}; 1.0×10^{-3}	4.3×10^{-3}; 5.5×10^{-3}	0.061; 0.071	2.9×10^{-5}; 3.4×10^{-5}	6.7×10^{-3}; 7.8×10^{-3}
σ_{tot} [d]	16; 20	0.45; 0.52	2.2; 2.7	33; 38	0.014; 0.016	3.6; 4.2

[a] The concentration of the simulated solution is 0.119 M, to scale to 1 M concentration, the average relaxation rate of the nuclei in bulk (the second solvation shell and more distant water molecules) is, therefore, divided by this number. [b] See Table 1. [c] The way to obtain these values is described in section 3.2.1. [d] The equation (9) is evaluated with σ_{tot}, the relaxation rate thus contains the effect of all combinations of the various cross-terms of σ. The relaxation rate is therefore larger than the sum of listed contributions.

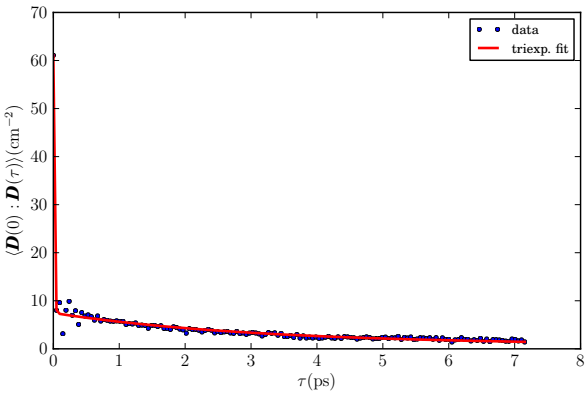

Fig. 1 Simulated time correlation function $\langle \boldsymbol{D}(0) : \boldsymbol{D}(\tau) \rangle$ of the zero-field splitting tensor of the aqueous solution of Ni^{2+}. The correlation function is calculated over 15625 snapshots (sampled over 0.75 ns) of the molecular dynamics trajectory. The correlation time obtained by integration of the fitted triexponential correlation function is $\tau_D = 1.15$ ps. The three components of the correlation function are likely to be associated with 1) a fast librational motion of the involved atoms 2) rotational motion of the water molecules, and 3) rotational motion of the $Ni^{2+}(H_2O)_6$ complex. The initial phases of the correlation function indicate an undersampling of the high frequency mode(s).

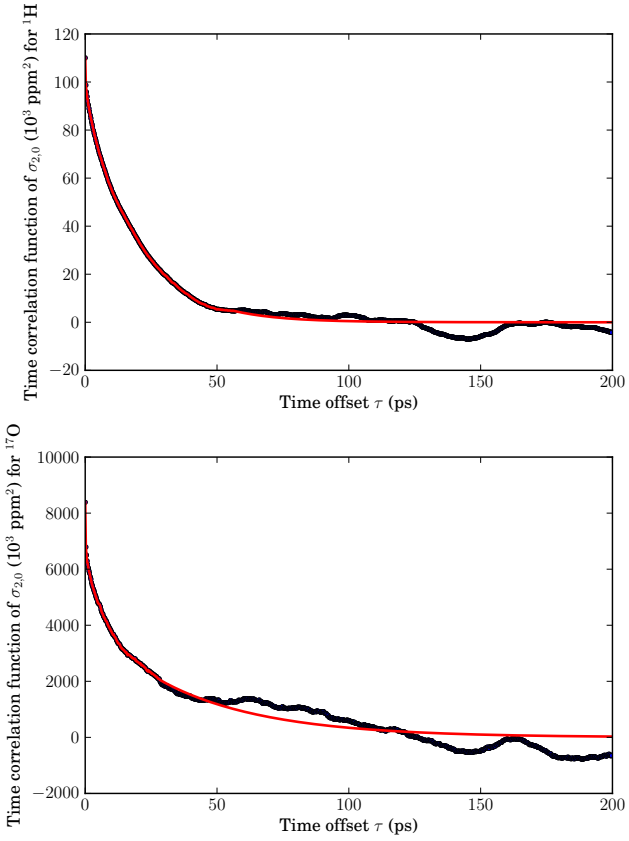

Fig. 2 Simulated time correlation function of the spherical $\sigma_{2,0}$ component of the shielding tensor for the ^{1}H (upper panel) and ^{17}O (lower panel) nuclei in the first solvation shell of $Ni^{2+}(aq)$. Calculated from 3125 snapshots sampled over 0.75 ns of molecular dynamics trajectory. The plots show the original data together with fitted biexponential (^{1}H) and triexponential (^{17}O) functions.

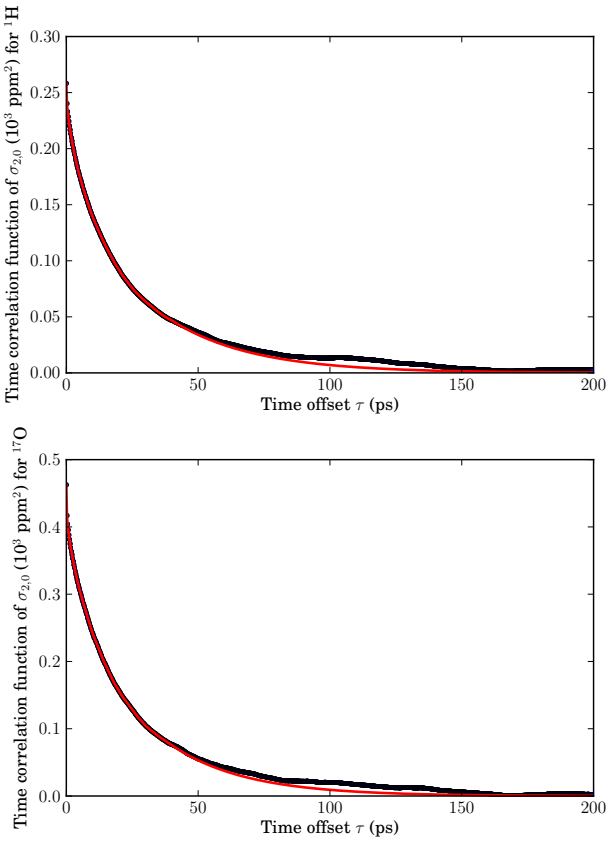

Fig. 3 As Figure 2 but for the bulk molecules beyond the first solvation shell. Biexponential functions were used for fitting the correlation functions of both nuclei.

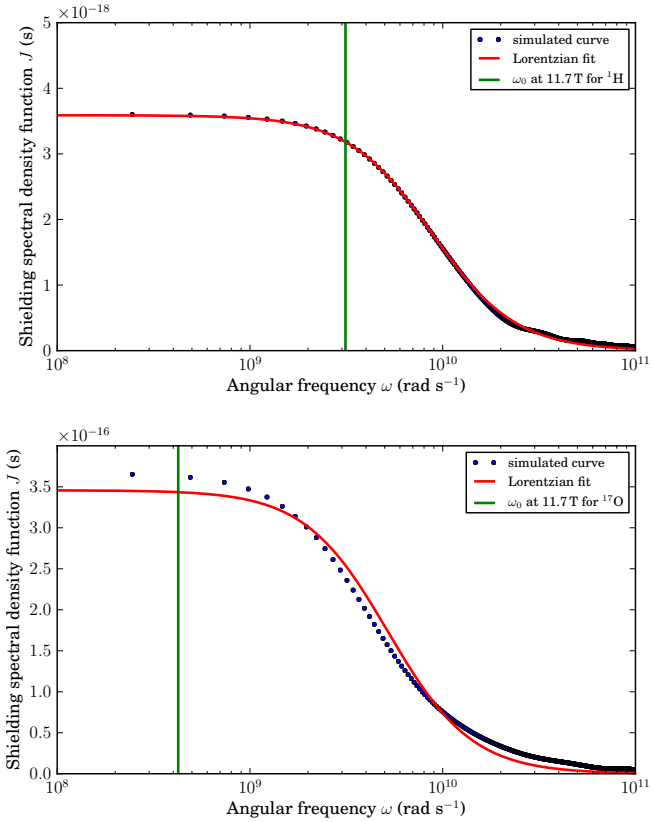

Fig. 4 The spectral density functions corresponding to the time correlation function of Figure 2, in which the noisy tail was replaced by a fitted function. The upper and lower panels are for ^{1}H and ^{17}O respectively. The red curve represents a fitted Lorentzian. The Larmor frequency of interest for the magnetic field of 11.7 T is marked by the green vertical line.

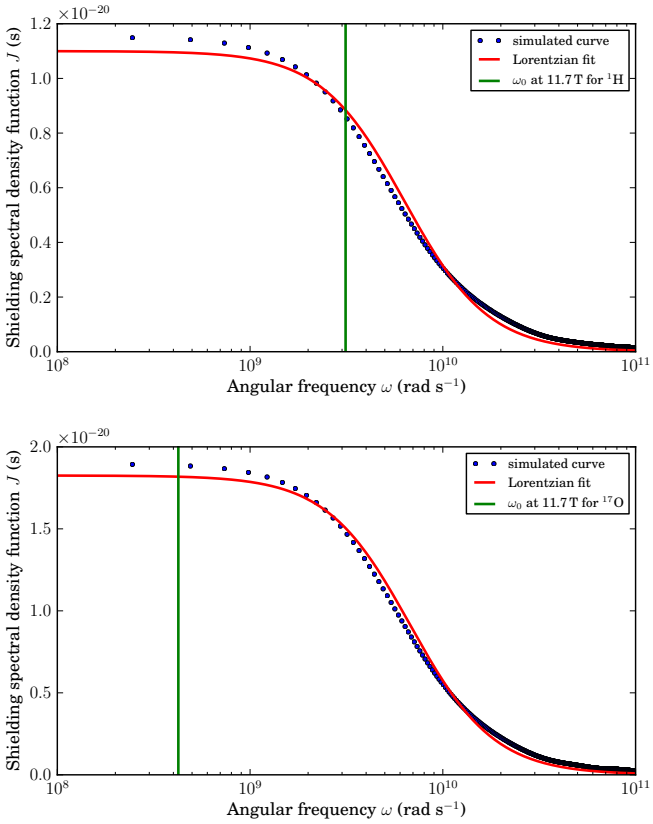

Fig. 5 As Figure 4 but for the bulk molecules.

Table 2 Calculated EPR and NMR parameters of the aqueous solution of Ni^{2+}. Average data from quantum-chemical calculations from MD simulation snapshots are shown, for both first and second solvation shell of the Ni^{2+} ion. Experimental results are listed where available.

	First shell	Second shell
g_{iso}	2.1021 ± 0.0002	–
g_{iso} (exp) [a]	2.25	–
Δ_5 (cm^{-1}) [b]	3.5	–
Δ_5 (cm^{-1}) (exp)	2.6,[c] 3.0[d]	–
$A_{con}(^1H)$	1.16 ± 0.03	0.0148 ± 0.0006
$A_{con}(^{17}O)$	-31.1 ± 0.1	-0.262 ± 0.004
$A_{dip,33}(^1H)$[e]	8.22 ± 0.01	1.530 ± 0.004
$A_{dip,33}(^{17}O)$[e]	-10.09 ± 0.02	-0.288 ± 0.001
Rh $[\boldsymbol{A}_{dip}(^1H)]$[f]	3.63 ± 0.03	0.06 ± 0.0003
Rh $[\boldsymbol{A}_{dip}(^{17}O)]$[f]	0.098 ± 0.0005	0.062 ± 0.001
$A_{iso}(^1H)$ [g]	1.13 ± 0.03	0.0146 ± 0.0004
$A_{iso}(^{17}O)$ [g]	-30.9 ± 0.1	-0.263 ± 0.004
$A_{iso}(^1H)$ (exp)	0.13 ± 0.01[h]	
$A_{iso}(^{17}O)$ (exp)	24,[i] -28.2[j]	
$\sigma^{iso}_{300K}(^1H)$	-83±2[k]	-1.09±0.04
$\sigma^{iso}_{300K}(^{17}O)$	-17288±40	-147±2
$\sigma^{iso}_{300K}(^1H)$ (exp)	10.3[k,l]	
$\sigma^{iso}_{300K}(^{17}O)$(exp)	-13582,[m] -12681[n]	

[a] Ref. [50] Measurement on hydrated Ni^{2+} salt crystals. This value has, however, been used also for Ni^{2+} solutions in the literature. [b] $\Delta_5 = \sqrt{\langle \boldsymbol{D} : \boldsymbol{D} \rangle / 5}$ the factor 5 is the number of the independent components needed to specify the ZFS-tensor. [c] Ref. [44] Electron spin relaxation study based on proton NMR relaxation measurement in aqueous Ni^{2+} solution. [d] Ref. [9] From proton NMR relaxation measurement in aqueous Ni^{2+} solution. [e] The largest (in absolute value) eigenvalue of the traceless tensor. [f] Rhombicity of the dipolar tensor, $\mathrm{Rh}(\boldsymbol{A}_{dip}) = A^{dip}_{22} - A^{dip}_{11}$. The values are very small for the oxygen nuclei in the six-fold-coordinated complex, in agreement with the nearly octahedral symmetry. [g] The isotropic value contains both the Fermi contact and spin-orbit contributions, the latter being much smaller. [h] Ref. [51]. [i] Ref. [52] The hyperfine coupling constant was reported without sign. [j] Ref. [53]. [k] The large discrepancy between computed and experimental values for the ^1H shielding constant is caused by the inaccuracy of the calculated hyperfine coupling constant A_{con} using the present DFT methods. The isotropic shielding constant does not contribute to the calculated relaxation rate, however. [l] This value of shielding constant was obtained by extrapolation of the experimental data measured in the range of 243.15–263.15 K [51] assuming an $\frac{1}{T}$ dependence of the paramagnetic chemical shifts. Furthermore, the reference was taken a pure water in gas phase (PBE), $\sigma_{ref,gas}(^1H) = 31.59$ ppm with a gas-to-liquid shift correction (B3LYP) $\delta_{gas\to liquid}(^1H) = -5.27$ ppm;[54] Orbital shielding of 25.7 ppm taken from Ref. [39] was further subtracted since in the present work the orbital shielding is not included in the results. [m] The value of the shielding constant was obtained by extrapolation of the experimental data measured in the range of 274.65–306.15 K [52] assuming an $\frac{1}{T}$ dependence of the paramagnetic chemical shifts. Referenced and corrected for gas-to-liquid shift as in footnote *l* using the values for ^{17}O: $\sigma_{ref,gas}(^{17}O) = 324.8$ ppm, $\delta_{gas\to liquid}(^{17}O) = -41.2$ ppm. Orbital shielding of 313 ppm from Ref. [39] was subtracted. [n] From the experimental data measured in the range of 243.65–308.15 K. [53] Referenced and corrected as in footnote *m*.

the corresponding contributions are 33 s^{-1} and 38 s^{-1}. In 1 M solution, the contributions of Curie relaxation by both first-solvation-shell nuclei and nuclei in bulk would be 2.2 s^{-1} and 2.7 s^{-1} (R_1 and R_2) for ^1H and 3.6 s^{-1} and 4.1 s^{-1} for ^{17}O nuclei. The accuracy of the results is expected to reside within 30% error limits for ^1H, which constitutes the primary object of interest for pNMR investigations. Conservative error limits for ^{17}O nuclei can amount up to 90%. For both nuclei in the present system, the experimental significance of these relaxation contributions is at the currently used magnetic fields negligible.

5 Acknowledgements

The research leading to these results has received funding from the *European Union* Seventh Framework Programme (FP7/2007-2013) under *grant agreement* n° 254552 (JM). Further support was received from Academy of Finland (JM, PL, JV), Tauno Tönning foundation (JV), and University of Oulu (JV). Computational resources due to CSC (Espoo, Finland) and the Finnish Grid Initiative project were used.

References

1 J. Kowalewski and L. Mäler, *Nuclear Spin Relaxation in Liquids: Theory, Experiments, and Applications*, Taylor & Francis, 1st edn, 2006, p. 440.
2 M. Luhmer and J. Reisse, *Prog. Nucl. Magn. Reson. Spectrosc.*, 1998, **33**, 57.
3 M. Hanni, P. Lantto and J. Vaara, *Phys. Chem. Chem. Phys.*, 2011, **13**, 13704.
4 A. G. Redfield, *IBM J. Res. Dev.*, 1957, **1**, 19.
5 A. G. Redfield, *Phys. Rev.*, 1965, **98**, 1787.
6 N. Bloembergen, *J. Chem. Phys.*, 1957, **27**, 572.
7 N. Bloembergen and L. O. Morgan, *J. Chem. Phys.*, 1961, **34**, 842.
8 J. Kowalewski, L. Nordenskiöld, N. Benetis and P. Westlund, *Prog. Nucl. Magn. Reson. Spectrosc.*, 1985, **17**, 141.
9 J. Kowalewski, T. Larsson and P. O. Westlund, *J. Magn. Reson.*, 1987, **74**, 56.
10 J. Kowalewski, C. Luchinat, T. Nilsson and G. Parigi, *J. Phys. Chem. A*, 2002, **106**, 7376.
11 D. Kruk, J. Kowalewski and P. Westlund, *J. Chem. Phys.*, 2004, **121**, 2215.
12 J. Kowalewski, D. Kruk and G. Parigi, *Adv. Inorg. Chem.*, 2005, **57**, 41.
13 J. Kowalewski, A. Egorov, D. Kruk, A. Laaksonen, S. N. Aski, G. Parigi and P. Westlund, *J. Magn. Reson.*, 2008, **195**, 103.
14 I. Bertini, O. Galas, C. Luchinat and G. Parigi, *J. Magn. Reson. Ser. A*, 1995, **113**, 151.
15 M. Odelius, C. Ribbing and J. Kowalewski, *J. Chem. Phys.*, 1996, **104**, 3181.
16 I. Bertini, C. Luchinat and G. Parigi, *Solution NMR of Paramagnetic Molecules: Applications to metallobiomolecules and models*, Elsevier Science, 1st edn, 2001, p. 376.
17 Z. Rinkevicius, J. Vaara, L. Telyatnyk and O. Vahtras, *J. Chem. Phys.*, 2003, **118**, 2550.
18 M. Gueron, *J. Magn. Reson.*, 1975, **19**, 58.
19 A. J. Vega and D. Fiat, *Mol. Phys.*, 1976, **31**, 347.
20 T. O. Pennanen and J. Vaara, *Phys. Rev. Lett.*, 2008, **100**, 133002.
21 S. Moon and S. Patchkovskii, in *Calculation of NMR and EPR Parameters: Theory and Applications*, ed. M. Kaupp, M. Bühl and V. G. Malkin, Wiley-VCH, 1st edn, 2004, p. 325.
22 T. O. Pennanen and J. Vaara, *J. Chem. Phys.*, 2005, **123**, 174102.
23 P. Ren and J. W. Ponder, *J. Phys. Chem. B*, 2003, **107**, 5933.
24 Unpublished results, forcefield parameters available on request from the authors.
25 F. Neese, *ORCA, Version 2.9*, 2012.
26 F. Neese, *J. Chem. Phys.*, 2005, **122**, 34107.
27 F. Neese, *J. Chem. Phys.*, 2003, **118**, 3939.
28 F. Neese, *J. Chem. Phys.*, 2007, **127**, 164112.
29 J. P. Perdew, K. Burke, M. Ernzerhof, *Phys. Rev. Lett.* **1996**, *77*, 3865, J. P. Perdew, K. Burke, M. Ernzerhof, *Phys. Rev. Lett.* **1997**, *78*, 1396; Erratum.
30 F. Neese, *J. Comput. Chem.*, 2003, **24**, 1740.
31 F. Weigend and R. Ahlrichs, *Phys. Chem. Chem. Phys.*, 2005, **7**, 3297.
32 C. Angeli, R. Cimiraglia and J.-P. Malrieu, *J. Chem. Phys.*, 2002, **117**, 9138.
33 C. Angeli, R. Cimiraglia and J.-P. Malrieu, *Chem. Phys. Lett.*, 2001, **350**, 297.
34 C. Angeli, R. Cimiraglia, S. Evangelisti, T. Leininger and J.-P. Malrieu, *J. Chem. Phys.*, 2001, **114**, 10252.
35 A. Kubica, J. Kowalewski, D. Kruk and M. Odelius, *J. Chem. Phys.*, 2013, **138**, 064304.
36 M. Munzarová and M. Kaupp, *J. Phys. Chem. A*, 1999, **103**, 9966.
37 F. Jensen, *J. Chem. Theory Comput.*, 2006, **2**, 1360.
38 A. Schäfer, H. Horn and R. Ahlrichs, *J. Chem. Phys.*, 1992, **97**, 2571.
39 J. Mareš, H. Liimatainen, T. O. Pennanen and J. Vaara, *J. Chem. Theory Comput.*, 2011, **7**, 3248.
40 N. F. Ramsey, *Phys. Rev.*, 1950, **78**, 699.
41 P. Hrobárik, R. Reviakine, A. V. Arbuznikov, O. L. Malkina, V. G. Malkin, F. H. Köhler and M. Kaupp, *J. Chem. Phys.*, 2007, **126**, 024107.
42 A. V. Arbuznikov, J. Vaara and M. Kaupp, *J. Chem. Phys.*, 2004, **120**, 2127.
43 S. Schmitt, P. Jost and C. van Wüllen, *J. Chem. Phys.*, 2011, **134**, 194113.
44 H. L. Friedman, M. Holz and H. G. Hertz, *J. Chem. Phys.*, 1979, **70**, 3369.
45 T. Helgaker and M. Jaszuński, *J. Chem. Theory Comput.*, 2007, **3**, 86.
46 A. Abragam, *The principles of nuclear magnetism*, Clarendon Press ; Oxford University Press, Oxford [Oxfordshire]; New York, 1983.
47 I. L. Moudrakovski, S. R. Breeze, B. Simard, C. I. Ratcliffe, J. A. Ripmeester, T. Seideman, J. S. Tse and G. Santyr, *J. Chem. Phys.*, 2001, **114**, 2173.
48 I. Bertini, F. Capozzi, C. Luchinat, G. Nicastro and Z. Xia, *J. Phys. Chem.*, 1993, **97**, 6351.
49 B. B. Garrett, A. B. Denison and S. W. Rabideau, *J. Phys. Chem.*, 1967, **71**, 2606.
50 J. H. E. Griffiths and J. Owen, *Proc. R. Soc. Lond. A*, 1952, **213**, 459.
51 J. Granot, *J. Chem. Phys.*, 1974, **61**, 3043.
52 J. W. Neely and R. E. Connick, *J. Am. Chem. Soc.*, 1972, **94**, 3419.
53 D. Fiat and A. M. Chmelnick, *J. Am. Chem. Soc.*, 1971, **93**, 2875.
54 T. S. Pennanen, J. Vaara, P. Lantto, A. Sillanpää, K. Laasonen and J. Jokisaari, *J. Am. Chem. Soc.*, 2004, **126**, 11093.

Magnetic field of the Curie spin manifests itself as both the pNMR shielding tensor and Curie relaxation, in analogy with CSA relaxation theory.